ACS APPLIED MATERIALS & INTERFACES

Research Article

www.acsami.org

Hollow Core–Shell SnO_2/C Fibers as Highly Stable Anodes for Lithium-Ion Batteries

Dan Zhou, Wei-Li Song, and Li-Zhen Fan*

Key Laboratory of New Energy Materials and Technologies, Institute of Advanced Materials and Technology, University of Science and Technology Beijing, Beijing 100083, China

Supporting Information

ABSTRACT: Given their competitive prospects for energy storage, lithium-ion batteries (LIBs) have attracted ever-intensive research interest. However, the large volume changes during cycling and structural pulverization significantly hinder the cycling stability and high capacity for lithium-alloy electrodes. Herein, novel one-dimensional (1D) hollow core–shell SnO_2/C fibers were synthesized by facile coaxial electrospinning. The as-prepared fibers that possess sufficient hollow voids and nanosized SnO_2 particles on the inner shell are able to serve as an anode in LIBs. The results suggest a reversible capacity of 1002 mAh g^{-1} (for the initial cycle at 100 mA g^{-1}), excellent rate capability, and a highly stable cycling performance with a discharge capacity of 833 mAh g^{-1} after 500 cycles at 600 mA g^{-1}. The superior electrochemical performance is attributed to the unique hollow core–shell structure, which offers sufficient voids for alleviating the volume changes of SnO_2 nanoparticles during lithiation/delithiation processes. The promising strategies and associated opportunities here demonstrate great potential in the fabrication of advanced anode materials for long-life LIBs.

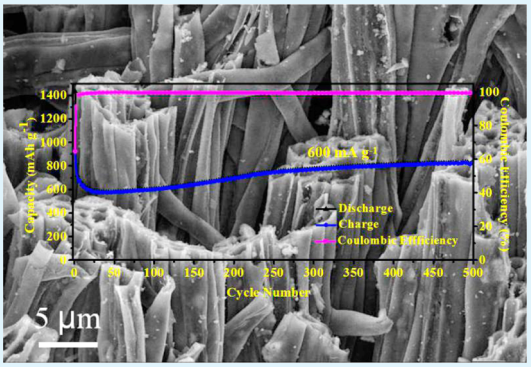

KEYWORDS: *lithium-ion batteries, anode, hollow core–shell, coaxial electrospinning, tin oxide, fibers*

INTRODUCTION

Driven by the high available energy density and constant emergence of suitable anode materials, lithium-ion batteries (LIBs) are widely used as a main energy power resource for the portable electronic terminals. Nowadays, attention has been paid to exploring sustainable, reliable, and large-scale energy storage for LIB systems as an alternative for fossil fuel power.[1−3] However, traditional graphite is limited by its low theoretical capacity (372 mAh g^{-1}),[4] and new lithium-alloy anodes suffer from the large volume changes during cycling and structural pulverization.[5−7] As a promising anode material, tin oxide (SnO_2) anode materials are of high theoretical capacity (782 mAh g^{-1}), low cost, low toxicity, and abundance.[8−10] However, similar to other investigated electrochemically active materials (e.g., Ge[11,12] and Si[13,14]), large volume change (~300%) caused by Li^+ insertion and extraction during the cycling process can always lead to pulverization, unstable solid electrolyte interphase (SEI), and weak electrical contact in SnO_2 materials, which results in severe capacity fade.[15−17] To solve the drawbacks, one feasible approach is to design various nanostructured materials (e.g., nanocrystallines, nanowires, nanospheres), and the absolute volume variation is reduced. For example, tin oxide nanocrystallines were synthesized using a sol–gel-assisted microwave method, and the reversible capacity for LIBs is as high as 900 mAh g^{-1}.[18] SnO_2 nanowires were prepared directly on the current collectors, and the battery delivered a high specific discharge capacity of 510 mAh g^{-1}.[19] SnO_2 hollow nanostructures were synthesized using a simple one-pot template-free process and demonstrated highly improved electrochemical properties in the fabricated LIBs.[20] Additionally, the introduction of other components is considered as another effective strategy to form SnO_2-based composites, which utilizes the merits of each component to enhance the electrochemical performance of the electrodes. Using a template-based sol–gel coating technique, Kim et al.[21] studied the SnO_2@Co_3O_4 hollow nanospheres as an LIB anode and acquired an enhanced reversible capacity of 962 mAh g^{-1} after 100 cycles. Zhu et al.[22] introduced TiO_2 nanotube@SnO_2 nanoflake arrays as an anode material and achieved a specific capacity of 498 mAhg g^{-1} at a high current density of 3.2 A g^{-1}. Hwa et al.[23] designed nano-Si/SnO_2 core–shell nanostructures as anodes and exhibited a reversible capacity of 1000 mAh g^{-1} with a good cycle retention of ~80% over 50 cycles. Besides, various SnO_2/carbon anodes, such as bowl-like SnO_2@carbon hollow particles,[24] SnO_2@carbon nanoclusters,[25] and SnO_2@C yolk–shell nanospheres,[26] with enhanced electrochemical properties have also been developed by confining SnO_2 material with mesoporous carbon. In a nutshell, effects have been done to design anode materials that can provide fast

Received: July 18, 2015
Accepted: September 8, 2015
Published: September 8, 2015

DOI: 10.1021/acsami.5b06512
ACS Appl. Mater. Interfaces 2015, 7, 21472−21478

electron transport, alleviate the volume change, stave off the capacity fading, and enhance the cycling stability.

Some novel one-dimensional (1D) materials based on core−shell structures have attracted great interest for the researchers.[27,28] Advanced designs have been applied to Sn/C,[29,30] Si/C,[31,32] and MnO_x/C[33] materials, and considerable improvements have been achieved. Such a 1D structure can provide more reactive sites for active materials and shorter diffusion paths for Li ions.[34,35] Furthermore, the voids in the 1D structure are also beneficial for the structural integrity. Therefore, 1D core−shell structures that integrate zero-dimensional SnO_2 nanoparticles (SnO_2 NPs) with carbon and preserve sufficient inner voids seem to be a promising structure for anode materials. In addition to the combined advantages of the nanoscaled SnO_2 and carbon, the most noticeable merit is the effective release of the volume expansion caused by SnO_2 lithiation.

In this work, hollow core−shell SnO_2/C fibers (denoted as core−shell SnO_2/C HFs) were fabricated by simple coaxial electrospinning. As expected, SnO_2 NPs were formed on the inner surface of the conductive hollow carbon shell, which combines the merits of nanoscaled SnO_2 with 1D core−shell structure, whereby the volume expansion of SnO_2 during lithiation/delithiation processes could be accommodated and the structure integrity would be maintained. The core−shell SnO_2/C HFs shows highly stability and excellent rate capability, with a superior capacity of up to 833 mAh g^{-1} after 500 cycles at 600 mA g^{-1}, revealing promising application for LIBs.

EXPERIMENTAL SECTION

Synthesis of SnO_2 NPs. SnO_2 NPs were prepared by a combined sol−gel and hydrothermal method. First, 3.506 g of $SnCl_4{\cdot}5H_2O$ was dissolved in 200 mL of deionized water as precursor solution, and 3 mL of a HCl solution was added to restrict the rapid hydrolysis of Sn^{4+}. Under vigorous magnetic stirring, a certain amount of a $NH_3{\cdot}H_2O$ solution was dripped slowly into the above solution until a pH value of 2 was achieved. When stirring was continued for 30 min, $Sn(OH)_4$ sol was formed, then centrifuged, and alternately washed with deionized water and ethyl alcohol. After that, impurity ions were removed and a white precipitate was collected. In the following, the precipitate was dispersed in deionized water for 30 min and then transferred to a 150 mL Teflon-lined autoclave. After heating at 160 °C for 12 h, the reactants were centrifuged and washed with ethyl alcohol. Finally, SnO_2 NPs were obtained followed by drying at 80 °C for 24 h.

Preparation of Core−Shell SnO_2/C HFs. In a typical synthesis, 0.24 g of SnO_2 NPs and 0.715 g of poly(methyl methacrylate) (PMMA; M_w = 996000, Sigma-Aldrich) were dissolved in a solution of 3 g of *N*,*N*-dimethylformamide (DMF) and 2 g of acetone, and the mixture was used as a core−shell. A total of 0.6 g of poly(acrylonitrile) (PAN; M_w = 150000, Sigma-Aldrich) was dissolved in 6 g of DMF, and the solution was used as a shell solution. Both of the above solutions were first treated by ultrasound for 30 min followed by vigorous magnetic stirring for 12 h. Hollow carbon fibers (denoted as carbon HFs) were prepared with the same method without adding SnO_2 NPs into the core solution. Each core and shell solution was transferred into a 5 mL of a plastic syringe, respectively. Both needles for the syringes had a diameter of 0.6 mm. In a coaxial electrospinning process, the voltage was supplied with 10 kV to form a jet flow, and the flow rates for the core and shell solutions were set at 0.025 and 0.033 mL min^{-1}, respectively. An aluminum foil was covered on the roller to collect the formed raw fibers. The distance between the needle and collector was 15 cm. The collected raw fibers were exposed to heat treatment in two stages: stabilization and carbonation. For stabilization, the raw fibers were placed in a muffle furnace and heated at 270 °C in air for 1 h. For carbonation, the stabilized fibers were calcined in a tubular furnace and conducted at 500 °C in an N_2 atmosphere for 3 h. The raising rates of the temperature for both stabilization and carbonation were 5 °C min^{-1}. After stabilization and carbonation, PMMA in the core of raw fibers was burned out, and core−shell SnO_2/C HFs were formed.

Characterizations. The crystal structure of as-synthesized samples was characterized by X-ray diffraction (XRD) on a Rigaku D/max-Rb X-ray diffractometer (Cu Kα, λ = 1.5406 Å, 40 kV, I = 150 mA). X-ray photoelectron spectroscopy (XPS) was performed on an EscaLab 250Xi electron spectrometer (Al Kα, spot size = 500 μm). Thermogravimetric analysis (TGA) was carried out by a Q600 simultaneous thermal analyzer (10 °C min^{-1}, air atmosphere). The morphology and microstructure images were observed by field-emission scanning electron microscopy (FE-SEM; JEOL JSM-6330) and high-resolution transmission electron microscopy (HR-TEM; JEM-2010F). The element distribution was recorded by energy-dispersive X-ray spectroscopy (EDS) through attachment on the JEOL-2010F microscope.

Electrochemical Measurements. Electrochemical characterization was conducted by using the two-electrode 2032-type coin cells. To prepare working electrodes, a slurry of active materials (SnO_2/C or SnO_2), carbon black, and poly(vinylidene fluoride) with a mass ratio of 80:10:10 in *N*-methylpyrrolidinone was uniformly coated on a copper foil and then dried in a vacuum oven at 70 °C for 24 h. Lithium metal was chosen as the counter electrode, and the separator was a Celgard 2400 polypropylene membrane. The electrolyte was 1 M $LiPF_6$ dissolved in ethylene carbonate, diethyl carbonate, and dimethyl carbonate (1:1:1 by volume). The whole assemble process for the cells was carried out in a glovebox under an argon atmosphere. The charge−discharge properties were tested between 0.01 and 3.0 V with a LAND CT2001A battery test system (Wuhan Land Electronic Co., China). Cyclic voltammetry (CV) and electrochemical impedance spectroscopy (EIS) tests were conducted with a CHI 660C electrochemical workstation (Shanghai Chenhua Co., China). CV was carried out between 0.01 and 3.0 V at a scanning rate of 0.2 mV s^{-1}, and EIS was measured in the frequency range between 0.01 Hz and 100 kHz with an amplitude of 5 mV. For comparison, bare SnO_2 NPs and carbon HFs were made as electrodes with the same process. All of the capacities reported in this work are based on the total mass of the SnO_2/C composite.

RESULTS AND DISCUSSION

Figure 1a illustrates the coaxial electrospinning process of core−shell SnO_2/C HFs. SnO_2 NPs, and PMMA in DMF/acetone (core solution) and PAN in DMF (shell solution) were pushed out under different flow rates. At the terminal of the electrospinning needles, the core solution was fully covered by the shell solution. Under high voltage, a taylor core was formed,

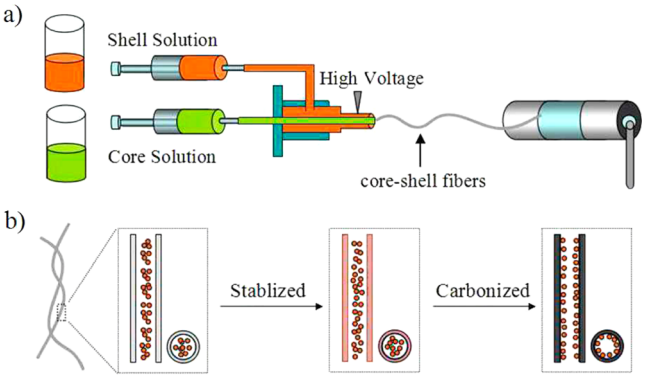

Figure 1. Schematic illustrations of (a) the coaxial electrospinning process for core−shell SnO_2/C HFs and (b) structural changes for core−shell SnO_2/C HFs during heat treatment.

DOI: 10.1021/acsami.5b06512
ACS Appl. Mater. Interfaces 2015, 7, 21472−21478

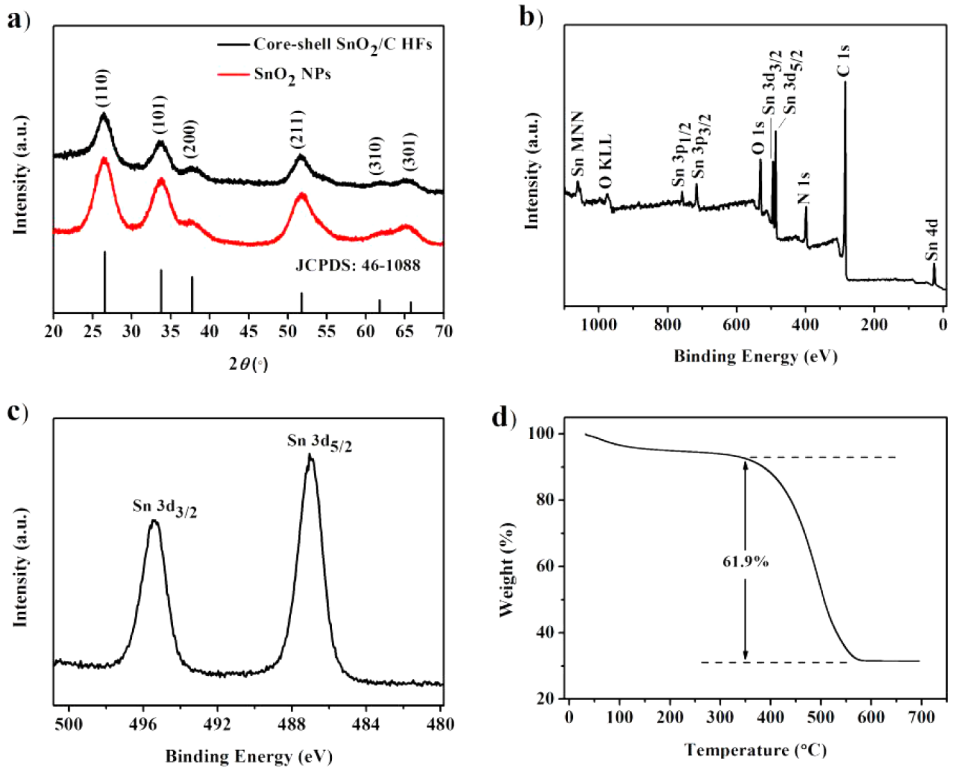

Figure 2. (a) XRD patterns, (b) XPS spectra, (c) Sn 3d XPS spectra, and (d) TGA of core−shell SnO_2/C HFs.

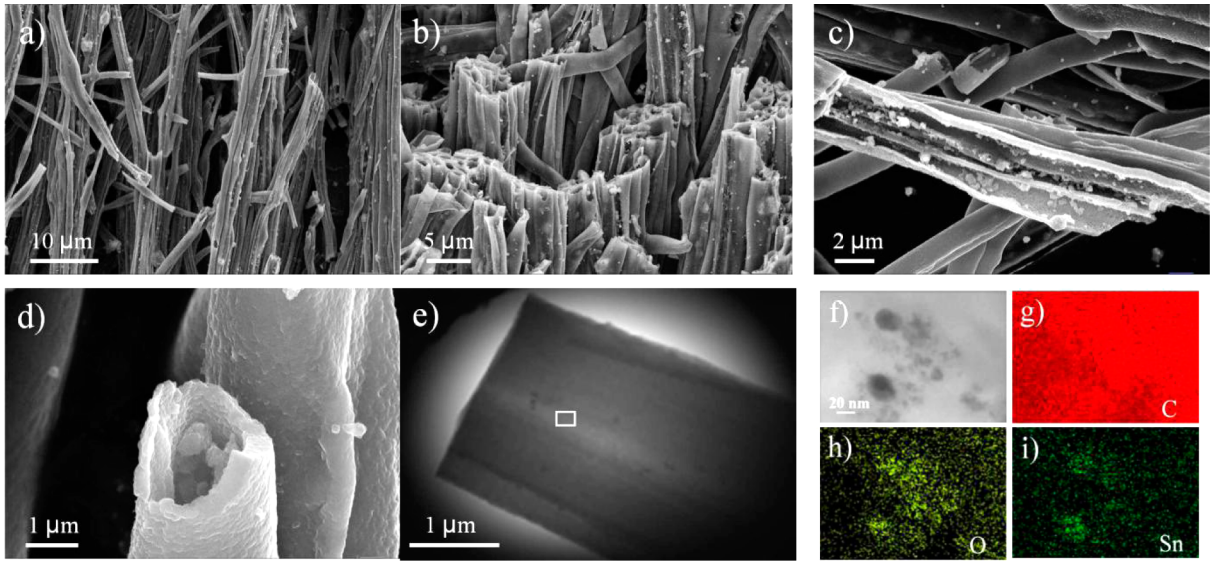

Figure 3. (a−d) FE-SEM images; (e) TEM image, and (f) HR-TEM image of core−shell SnO_2/C HFs and (g−i) EDS mapping of carbon, oxygen, and tin elements.

followed by a jet flow to the collector to produce solid-state composite fibers. The as-produced fibers were so-called raw fibers. Next, the raw fibers were exposed to stabilization (270 °C in air) and carbonization (500 °C in air) processes successively. PAN could remain stable and eventually form the carbon shell of the fibers. Meanwhile, PMMA in the core was decomposed, and SnO_2 NPs were immobilized on the inner carbon shell, leaving sufficient hollow voids in the fibers (Figure 1b). Thus, core−shell SnO_2/C HFs were formed.

XRD patterns of as-prepared samples are shown in Figure 2a. Core−shell SnO_2/C HFs and SnO_2 NPs are well assigned to tetragonal SnO_2 (JCPDS 46-1088). The locations of their characteristic peaks are nearly identical, which indicates that the shell of core−shell SnO_2/C HFs is amorphous carbon. Further analyzed by XPS (Figure 2b), the core−shell SnO_2/C HFs mainly contain carbon, oxygen, and tin (slight amount of nitrogen derived from the PAN precursor). In the Sn 3d XPS spectra, two peaks derived from Sn $3d_{3/2}$ and $3d_{5/2}$ suggest binding energies of 495.63 and 487.2 eV, respectively (Figure 2c),[36,37] implying that SnO_2 NPs were formed in core−shell SnO_2/C HFs. TGA was carried out to identify the contents of SnO_2 and carbon in core−shell SnO_2/C HFs. As shown in

DOI: 10.1021/acsami.5b06512
ACS Appl. Mater. Interfaces 2015, 7, 21472−21478

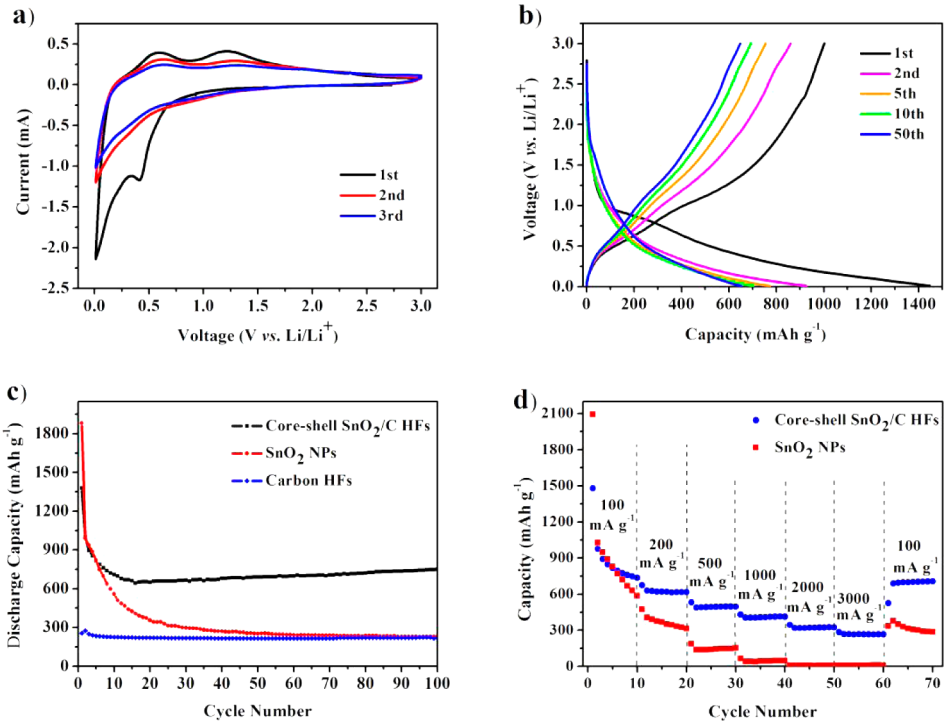

Figure 4. Electrochemical performances: (a) CV curves of core−shell SnO_2/C HF electrodes; (b) charge−discharge curves of core−shell SnO_2/C HF electrodes at a current density of 100 mA g^{-1}; (c) cycling performance of core−shell SnO_2/C HF, bare SnO_2 NP, and pristine carbon HF electrodes at a current density of 100 mA g^{-1}; (d) rate capability of core−shell SnO_2/C HF and bare SnO_2 NP electrodes at various current densities.

Figure 2d, a slight weight loss below 350 °C in the TGA curve is attributed to the loss of water and small molecules. The dramatic weight reduction between 350 and 550 °C is assigned to carbon decomposition under an air atmosphere, indicating that the carbon concentration in the core−shell SnO_2/C HFs is about 61.9% and thus the SnO_2 concentration is 38.1%.

FE-SEM images of core−shell SnO_2/C HFs are shown in Figure 3a−d, which presents hollow tubular fibers with an average diameter of 2 μm and about 50−100 nm shell thickness. SnO_2 NPs and clusters were found to be attached on the inner shell, which makes sufficient hollow voids in the 1D core−shell SnO_2/C HFs. Moreover, the hollow structure for pristine carbon HFs (Figure S1) reveals the same feature in core−shell SnO_2/C HFs. Figure 3e is the TEM image of core−shell SnO_2/C HFs, which further confirms the formation of a hollow structure. EDS mapping images (Figure 3f−i) demonstrate the distribution of carbon and tin elements in the selected region in Figure 3f, indicating that the carbon, oxygen, and tin patterns are in good agreement with those of the observed SnO_2 NPs and clusters in the inner shell of core−shell SnO_2/C HFs in Figure 3f. The sufficient hollow voids in the core−shell SnO_2/C HFs are conducive to alleviating the volume expansion of SnO_2 during the lithiation process, and the 1D carbon shells are favorable in the generation of three-dimensional conductive networks for substantially improving the electronic transport paths. In addition, the unique 1D core−shell structure is beneficial for the structural integrity, thus facilitating the formation of stable SEI layers.[31−35] It should be noted that the mass ratio of carbon and attached SnO_2 NPs would directly impact the electrochemical properties of electrodes because a relatively low content of carbon or a high content of SnO_2 can increase the capacity of the core−shell SnO_2/C HFs. On the contrary, insufficient SnO_2 NPs will significantly reduce the capacity (which leads to low volumetric capacity and power density). Thus, accommodating the component ratio in precursor solutions and rationally controlling the thickness of the carbon shell would be two feasible approaches.

The electrochemical performance of the core−shell SnO_2/C HFs as anode materials for LIBs was demonstrated in Figure 4. Figure 4a gives the CV curves of core−shell SnO_2/C HF electrode for the first three cycles. Two pronounced peaks were observed at 0.928 and 0.409 V in the first cathodic scanning. The former corresponds to the reduction of SnO_2 to Sn along with the formation of a SEI layer;[10,38,39] The latter is attributed to the alloying of lithium with tin (Li_xSn) and the formation of Li_xC_6.[10,39] According to the anodic scanning, two obvious oxidation peaks are located at 1.225 and 0.607 V in the first cycle, which correspond to the reversible extraction of lithium from Li_xSn and Li_xC_6,[38,39] respectively. In the subsequent two cycles, the CV curves kept fairly stable and no obvious changes were observed, indicating the good cycling stability of core−shell SnO_2/C HF electrodes. Figure 4b shows the charge−discharge curves of core−shell SnO_2/C HF electrodes for the 1st, 2nd, 5th, 10th, and 50th cycles at a current density of 100 mA g^{-1}. The initial charge and discharge capacities of the core−shell SnO_2/C HF electrodes are 1002 and 1446 mAh g^{-1}, with a Coulombic efficiency of 69.3%. The irreversible capacity loss of 444 mAh g^{-1} in the first cycle is attributed to the formation of SEI layers on the surface of core−shell SnO_2/C HFs. In subsequent cycles, the discharge curves are almost overlapped and core−shell SnO_2/C HF electrodes deliver discharge capacities of 926, 772, 702, and 652 mAh g^{-1} in the 2nd, 5th, 10th, and 50th cycles, respectively, with the Coulombic efficiency close to 100%. Figure 4c shows the cycling performance of the core−shell SnO_2/C HFs, bare SnO_2 NPs,

DOI: 10.1021/acsami.5b06512
ACS Appl. Mater. Interfaces 2015, 7, 21472−21478

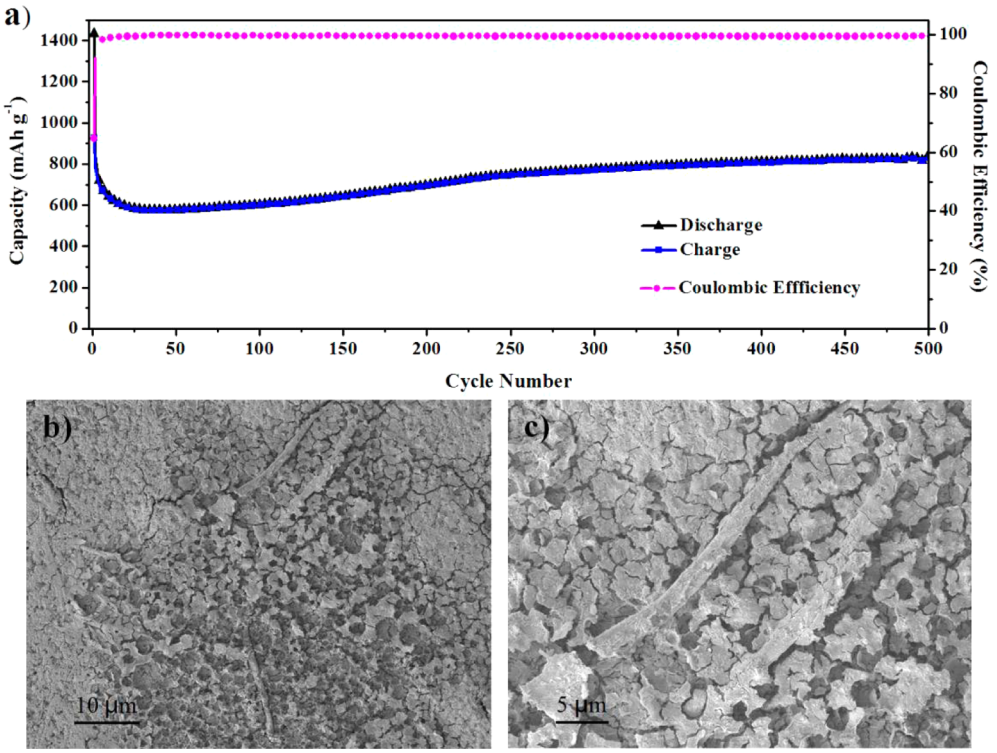

Figure 5. (a) Cycling performance of core−shell SnO_2/C HF electrodes at a current density of 600 mA g^{-1}. (b and c) FE-SEM images of core−shell SnO_2/C HF electrodes after 500 cycles at a current density of 600 mA g^{-1}.

and carbon HF electrodes at a current density of 100 mA g^{-1}. Core−shell SnO_2/C HF electrodes deliver capacity decay before the 17th cycle because of the formation of stable SEI layers.[10,38,39] In subsequent cycles, the capacity gradually increased and reached 750 mAh g^{-1} after 100 cycles. The capacity increase for the core−shell SnO_2/C HF electrodes was mainly attributed to the delay contact between the active materials and electrolytes.[10,40] SnO_2 NPs in core−shell SnO_2/C HFs would be reconstructed upon repeated cycles and may improve the contact between active materials and electrolytes, leading to fully activated materials and enhanced capacity. A similar phenomenon is also demonstrated in other reports.[10,33,41] In contrast, bare SnO_2 NP electrodes presented severe capacitive fade in the whole cycling process. Figure 4d plots a comparison of the rate capability between the core−shell SnO_2/C HFs and bare SnO_2 NP electrodes at various current densities, implying that core−shell SnO_2/C HFs show more improved rate capability than the bare SnO_2 NPs. The discharge capacities were found to be 736, 617, 495, 413, 325, and 267 mAh g^{-1} at current densities of 100, 200, 500, 1000, 2000, and 3000 mA g^{-1}, respectively. When the current density went back to 100 mA g^{-1}, a higher capacity of 707 mAh g^{-1} was obtained, revealing good capacity recovery. Compared to the bare SnO_2 NPs, much lower charge-transfer resistance R_{ct} was observed in the core−shell SnO_2/C HFs (149.7 and 90.2 Ω), displaying good electrochemical kinetics in the electrode (Figure S2) . Because of the electrically conductive feature, the carbonized shell contributed to improvement of the electronic transport and electrochemical activity of the core−shell SnO_2/C HFs.

It is emphasized that the core−shell SnO_2/C HF electrodes show a superior cycling stability at a current density of 600 mA g^{-1}. As shown in Figure 5a, the discharge capacity of core−shell SnO_2/C HFs is 575 mAh g^{-1} after the initial 35 cycles. The discharge capacity increased gradually and remained stable after 220 cycles. The core−shell SnO_2/C HF anode was able to remain stable up to 500 cycles and approach an excellent capacity as high as 833 mAh g^{-1}. Such superior stability promises a long life cycle for LIBs. To study the morphology of the core−shell SnO_2/C HFs after 500 cycles, the electrode was soaked in a dimethylcarbonate solution for 12 h, combined with drying in a vacuum oven at 50 °C for 10 h. Although slight structural changes were observed, the core−shell SnO_2/C HFs retained the integrity after 500 cycles, demonstrating the accommodation of the core−shell SnO_2/C HFs for large volume change (Figure 5b,c).

Compared with recently reported SnO_2/C materials, the core−shell SnO_2/C HFs in this work exhibited considerably enhanced cycling stability, excellent rate capability, and long life cycle (Table 1[26,42−50]). The possible reasons are mainly as follows. First, nanoscaled SnO_2 and sufficient hollow voids formed by the proper content of SnO_2 NPs on the inner surface of the conductive hollow carbon shell allow the composite SnO_2/C HFs to effectively alleviate the volume expansion of SnO_2 NPs during cycles, which essentially improves the structural integrity. Second, the conductive hollow carbon shell is conducive to the electronic transport and electrochemical activity of the core−shell SnO_2/C HFs. Thus, excellent electrochemical performances were obtained.

CONCLUSION

In summary, SnO_2/C HFs were synthesized by using a simple coaxial electrospinning method. Such a unique design offers the as-prepared SnO_2/C HFs to provide sufficient hollow voids to effectively accommodate the volume expansion of SnO_2 NPs during cycles, which maintains the structural integrity and also facilitates the electronic transport and electrochemical activity. Thus, the conductive composite SnO_2/C HFs demonstrated a

DOI: 10.1021/acsami.5b06512
ACS Appl. Mater. Interfaces 2015, 7, 21472−21478

Table 1. Comparison of the Electrochemical Properties of Core–Shell SnO_2/C HFs with Recently Reported SnO_2/C Anode Materials for LIBs

sample	current density (mA g^{-1})	no. of cycles	capacity (mAh g^{-1})	ref/year
20SnO_2@OMC	100	100	593	42/2013
double-void-space SnO_2/carbon	100	50	408	43/2013
SnO_2@C yolk–shell nanospheres	100	100	630	26/2014
SnO_2(57)-C hybrid	500	50	630	44/2014
SnO_2@C yolk–shell spheres	100	30	512	45/2014
SnO_2@C nanofibers	80	100	411	46/2014
SnO_2/mesoporous carbon composites	200	300	573	47/2014
nano-SnO_2/C composite	500	420	640	48/2014
SnO_2/C hybrid triple-type nanosphere	300	350	653	49/2015
SnO_2@ C mesoporous carbon	100	100	600	50/2015
core–shell SnO_2/C HFs	100	100	750	
	600	500	833	our work

high reversible capacity and excellent rate capability. The superior cycling performance suggests that such a hollow core–shell structure for composite fibers could also be extended to other related electrodes for achieving advanced energy storage devices.

■ ASSOCIATED CONTENT

Supporting Information

The Supporting Information is available free of charge on the ACS Publications website at DOI: 10.1021/acsami.5b06512.

FE-SEM image of carbon HFs and Nyquist plots of core–shell SnO_2/C HFs and SnO_2 NP electrodes after 20 cycles (PDF)

■ AUTHOR INFORMATION

Corresponding Author

*Tel./fax: +86 10 62334311. E-mail: fanlizhen@ustb.edu.cn (L.-Z.F.).

Author Contributions

All authors have given approval to the final version of the manuscript.

Notes

The authors declare no competing financial interest.

■ ACKNOWLEDGMENTS

Financial support from the 973 projects (2015CB932500 and 2013CB934001) and the NSF of China (Grants 51172024, 51372022, and 51302011) is gratefully acknowledged.

■ REFERENCES

(1) Dunn, B.; Kamath, H.; Tarascon, J. M. Electrical Energy Storage for the Grid: A Battery of Choices. *Science* **2011**, *334*, 928–935.

(2) Yang, Z. G.; Zhang, J. L.; Kintner-Meyer, M. C. W.; Lu, X. C.; Choi, D.; Lemmon, J. P.; Liu, J. Electrochemical Energy Storage for Green Grid. *Chem. Rev.* **2011**, *111*, 3577–3613.

(3) Armand, M.; Tarascon, J. M. Researchers Must Find A Sustainable Way of Providing the Power Our Modern Lifestyles Demand. *Nature* **2008**, *451*, 652–657.

(4) Tarascon, J. M.; Armand, M. Issues and Challenges Facing Rechargeable Lithium Batteries. *Nature* **2001**, *414*, 359–367.

(5) Obrovac, M. N.; Chevrier, V. L. Alloy Negative Electrodes for Li-Ion Batteries. *Chem. Rev.* **2014**, *114*, 11444–11502.

(6) Park, C. M.; Kim, J. H.; Kim, H.; Sohn, H. J. Li-Alloy Based Anode Materials for Li Secondary Batteries. *Chem. Soc. Rev.* **2010**, *39*, 3115–3141.

(7) Goodenough, J. B.; Park, K. S. The Li-Ion Rechargeable Battery: A Perspective. *J. Am. Chem. Soc.* **2013**, *135*, 1167–1176.

(8) Zhou, X. S.; Wan, L. J.; Guo, Y. G. Binding SnO_2 Nanocrystals in Nitrogen-Doped Graphene Sheets as Anode Materials for Lithium-Ion Batteries. *Adv. Mater.* **2013**, *25*, 2152–2157.

(9) Ding, Y. L.; Wen, Y. R.; van Aken, P. A.; Maier, J.; Yu, Y. Large-Scale Low Temperature Fabrication of SnO_2 Hollow/Nanoporous Nanostructures: The Template-Engaged Replacement Reaction Mechanism and High-Rate Lithium Storage. *Nanoscale* **2014**, *6*, 11411–11418.

(10) Zhou, X. S.; Dai, Z. H.; Liu, S. H.; Bao, J. C.; Guo, Y. G. Ultra-Uniform SnO_x/ Carbon Nanohybrids toward Advanced Lithium-Ion Battery Anodes. *Adv. Mater.* **2014**, *26*, 3943–3949.

(11) Liu, J.; Song, K. P.; Zhu, C. B.; Chen, C. C.; van Aken, P. A.; Maier, J.; Yu, Y. Ge/C Nanowires as High-Capacity and Long-Life Anode Materials for Li-Ion Batteries. *ACS Nano* **2014**, *8*, 7051–7059.

(12) Xue, D. J.; Xin, S.; Yan, Y.; Jiang, K. C.; Yin, Y. X.; Guo, Y. G.; Wan, L.-J. Improving the Electrode Performance of Ge through Ge@C Core-Shell Nanoparticles and Graphene Networks. *J. Am. Chem. Soc.* **2012**, *134*, 2512–2515.

(13) Wang, M. S.; Song, W. L.; Wang, J.; Fan, L. Z. Highly Uniform Silicon Nanoparticle/Porous Carbon Nanofiber Hybrids towards Free-Standing High-Performance Anodes for Lithium-Ion Batteries. *Carbon* **2015**, *82*, 337–345.

(14) Zhou, X. S.; Yin, Y. X.; Wan, L. J.; Guo, Y. G. Self-Assembled Nanocomposite of Silicon Nanoparticles Encapsulated in Graphene through Electrostatic Attraction for Lithium-Ion Batteries. *Adv. Energy. Mater.* **2012**, *2*, 1086–1090.

(15) Gurunathan, P.; Ette, P. M.; Ramesha, K. Synthesis of Hierarchically Porous SnO_2 Microspheres and Performance Evaluation as Li-Ion Battery Anode by Using Different Binders. *ACS Appl. Mater. Interfaces* **2014**, *6*, 16556–16564.

(16) Zhang, L.; Zhang, G. Q.; Wu, H. B.; Yu, L.; Lou, X. W. Hierarchical Tubular Structures Constructed by Carbon-Coated SnO_2 Nanoplates for Highly Reversible Lithium Storage. *Adv. Mater.* **2013**, *25*, 2589–2593.

(17) Dong, Y. F.; Zhao, Z. B.; Wang, Z. Y.; Liu, Y.; Wang, X. Z.; Qiu, J. S. Dually Fixed SnO_2 Nanoparticles on Graphene Nanosheets by Polyaniline Coating for Superior Lithium Storage. *ACS Appl. Mater. Interfaces* **2015**, *7*, 2444–2451.

(18) Subramanian, V.; Burke, W. W.; Zhu, H. W.; Wei, B. Q. Novel Microwave Synthesis of Nanocrystalline SnO_2 and Its Electrochemical Properties. *J. Phys. Chem. C* **2008**, *112*, 4550–4556.

(19) Ko, Y. D.; Kang, J. G.; Park, J. G.; Lee, S. J.; Kim, D. W. Self-Supported SnO_2 Nanowire Electrodes for High-Power Lithium-Ion Batteries. *Nanotechnology* **2009**, *20*, 455701–455706.

(20) Lou, X. W.; Wang, Y.; Yuan, C. L.; Lee, J. Y.; Archer, L. A. Template-Free Synthesis of SnO_2 Hollow Nanostructures with High Lithium Storage Capacity. *Adv. Mater.* **2006**, *18*, 2325–2329.

(21) Kim, W. S.; Hwa, Y.; Kim, H. C.; Choi, J. H.; Sohn, H. J.; Hong, S. H. SnO_2@Co_3O_4 Hollow Nano-Spheres for a Li-ion Battery Anode with Extraordinary Performance. *Nano Res.* **2014**, *7*, 1128–1136.

(22) Zhu, C. R.; Xia, X. H.; Liu, J. L.; Fan, Z. X.; Chao, D. L.; Zhang, H.; Fan, H. J. TiO_2 nanotube@SnO_2 Nanoflake Core–Branch Arrays for Lithium-ion Battery Anode. *Nano Energy* **2014**, *4*, 105–112.

(23) Hwa, Y.; Kim, W. S.; Yu, B. C.; Kim, H. S.; Hong, S. H.; Sohn, H. J. Reversible Storage of Li-ion in Nano-Si/SnO_2 Core–Shell Nanostructured Electrode. *J. Mater. Chem. A* **2013**, *1*, 3733–3738.

DOI: 10.1021/acsami.5b06512
ACS Appl. Mater. Interfaces 2015, 7, 21472–21478

(24) Liang, J.; Yu, X. Y.; Zhou, H.; Wu, H. B.; Ding, S. J.; Lou, X. W. Bowl-like SnO_2@Carbon Hollow Particles as an Advanced Anode Material for Lithium-Ion Batteries. *Angew. Chem., Int. Ed.* **2014**, *53*, 12803−12807.
(25) He, M.; Yuan, L. X.; Hu, X. L.; Zhang, W. X.; Shu, J.; Huang, Y. H. A SnO_2@Carbon Nanocluster Anode Material with Superior Cyclability and Rate Capability for Lithium-Ion Batteries. *Nanoscale* **2013**, *5*, 3298−3305.
(26) Wang, J. X.; Li, W.; Wang, F.; Xia, Y. Y.; Asiri, A. M.; Zhao, D. Y. Controllable Synthesis of SnO_2@C Yolk−Shell Nanospheres as a High-Performance Anode Material for Lithium Ion Batteries. *Nanoscale* **2014**, *6*, 3217−3222.
(27) Zhang, B. H.; Yu, X. Y.; Ge, C. Y.; Dong, X. M.; Fang, Y. P.; Li, Z. S.; Wang, H. Q. Novel 3-D Superstructures Made Up of SnO_2@C Core-Shell Nanochains for Energy Storage Applications. *Chem. Commun.* **2010**, *46*, 9188−9190.
(28) Zhong, Y.; Li, X. F.; Zhang, Y.; Li, R. Y.; Cai, M.; Sun, X. L. Nanostructued Core−Shell Sn Nanowires@CNTs with Controllable Thickness of CNT Shells for Lithium Ion Battery. *Appl. Surf. Sci.* **2015**, *332*, 192−197.
(29) Yu, Y.; Gu, L.; Wang, C.; Dhanabalan, A.; van Aken, P. A.; Maier, J. Encapsulation of Sn@carbon Nanoparticles in Bamboo-Like Hollow Carbon Nanofibers as An Anode Material in Lithium-Based Batteries. *Angew. Chem., Int. Ed.* **2009**, *48*, 6485−6489.
(30) Yu, Y.; Gu, L.; Zhu, C.; van Aken, P. A.; Maier, J. Tin Nanoparticles Encapsulated in Porous Multichannel Carbon Microtubes: Preparation by Single-Nozzle Electrospinning and Application as Anode Material for High-Performance Li-Based Batteries. *J. Am. Chem. Soc.* **2009**, *131*, 15984−15985.
(31) Hwang, T. H.; Lee, Y. M.; Kong, B. S.; Seo, J. S.; Choi, J. W. Electrospun Core−Shell Fibers for Robust Silicon Nanoparticle-Based Lithium Ion Battery Anodes. *Nano Lett.* **2012**, *12*, 802−807.
(32) Lee, B. S.; Son, S. B.; Park, K. M.; Seo, J. H.; Lee, S. H.; Choi, I. S.; Oh, K. H.; Yu, W. R. Fabrication of Si Core/C Shell Nanofibers and Their Electrochemical Performances as a Lithium-Ion Battery Anode. *J. Power Sources* **2012**, *206*, 267−273.
(33) Cai, Z. Y.; Xu, L.; Yan, M. Y.; Han, C. H.; He, L.; Hercule, K. M.; Niu, C. J.; Yuan, Z. F.; Xu, W. W.; Qu, L. B.; Zhao, K. N.; Mai, L. Q. Manganese Oxide/Carbon Yolk−Shell Nanorod Anodes for High Capacity Lithium Batteries. *Nano Lett.* **2015**, *15*, 738−744.
(34) Mai, L. Q.; Tian, X. C.; Xu, X.; Chang, L.; Xu, L. Nanowire Electrodes for Electrochemical Energy Storage Devices. *Chem. Rev.* **2014**, *114*, 11828−11862.
(35) Su, L. W.; Jing, Y.; Zhou, Z. Li Ion Battery Materials with Core−Shell Nanostructures. *Nanoscale* **2011**, *3*, 3967−3983.
(36) Li, L.; Kovalchuk, A.; Tour, J. M. SnO_2-Reduced Graphene Oxide Nanoribbons as Anodes for Lithium Ion Batteries with Enhanced Cycling Stability. *Nano Res.* **2014**, *7*, 1319−1326.
(37) Yang, Z. X.; Du, G. D.; Guo, Z. P.; Yu, X. B.; Chen, Z. X.; Guo, T. L.; Zeng, R. Encapsulation of TiO_2(B) Nanowire Cores into SnO_2/Carbon Nanoparticle Shells and Their High Performance in Lithium Storage. *Nanoscale* **2011**, *3*, 4440−4447.
(38) Li, S. Y.; Xie, W. H.; Wang, S. Y.; Jiang, X. Y.; Peng, S. L.; He, D. Y. Facile Synthesis of rGO/SnO_2 Composite Anodes for Lithium Ion Batteries. *J. Mater. Chem. A* **2014**, *2*, 17139−17145.
(39) Chen, L. B.; Yin, X. M.; Mei, L.; Li, C. C.; Lei, D. N.; Zhang, M.; Li, Q. H.; Xu, Z.; Xu, C. M.; Wang, T. H. Mesoporous SnO_2@Carbon Core−Shell Nanostructures with Superior Electrochemical Performance for Lithium Ion Batteries. *Nanotechnology* **2012**, *23*, 035402−035407.
(40) Wu, H.; Yu, G.; Pan, L.; Liu, N.; McDowell, M. T.; Bao, Z.; Cui, Y. Stable Li-ion Battery Anodes by In-Situ Polymerization of Conducting Hydrogel to Conformally Coat Silicon Nanoparticles. *Nat. Commun.* **2013**, *4*, 1943−1948.
(41) Cong, H. P.; Xin, S.; Yu, S. H. Flexible Nitrogen-Doped Graphene/SnO_2 Foams Promise Kinetically Stable Lithium Storage. *Nano Energy* **2015**, *13*, 482−490.
(42) Wang, X. K.; Li, Z. Q.; Yin, L. W. Nanocomposites of SnO_2@Ordered Mesoporous Carbon (OMC) As Anode Materials for Lithium-ion Batteries with Improved Electrochemical Performance. *CrystEngComm* **2013**, *15*, 7589−7597.
(43) Wang, W. C.; Li, P. H.; Fu, Y. B.; Ma, X. H. The Preparation of Double-Void-Space SnO_2/Carbon Composite as High-Capacity Anode Materials for Lithium-Ion Batteries. *J. Power Sources* **2013**, *238*, 464−468.
(44) Qu, W. H.; Han, F.; Lu, A. H.; Xing, C.; Qiao, M.; Li, W. C. Combination of a SnO_2−C Hybrid Anode and a Tubular Mesoporous Carbon Cathode in a High Energy Density Non-Aqueous Lithium Ion Capacitor: Preparation and Characterization. *J. Mater. Chem. A* **2014**, *2*, 6549−6557.
(45) Li, J. P.; Wu, P.; Ye, Y.; Wang, H.; Zhou, Y. M.; Tang, Y. W.; Lu, T. H. Designed Synthesis of SnO_2@C Yolk-Shell Spheres for High-Performance Lithium Storage. *CrystEngComm* **2014**, *16*, 517−521.
(46) Fu, Z. R.; Li, X. F.; Xu, G. R. Novel Electrospun SnO_2@Carbon Nanofibers As High Performance Anodes for Lithium-Ion Batteries. *Cryst. Res. Technol.* **2014**, *49*, 441−445.
(47) Raju, V.; Wang, X. F.; Luo, W.; Ji, X. L. Multiple Ambient Hydrolysis Deposition of Tin Oxide into Nanoporous Carbon To Give a Stable Anode for Lithium-Ion Batteries. *Chem. - Eur. J.* **2014**, *20*, 7686−7691.
(48) Fan, X. L.; Shao, J.; Xiao, X. Z.; Wang, X. H.; Li, S. Q.; Ge, H. W.; Chen, L. X.; Wang, C. S. In situ Synthesis of SnO_2 Nanoparticles Encapsulated in Micro/Mesoporous Carbon Foam as a High-Performance Anode Material for Lithium Ion Batteries. *J. Mater. Chem. A* **2014**, *2*, 18367−18374.
(49) Hu, H.; Cheng, H. Y.; Li, G. J.; Liu, J. P.; Yu, Y. Design of SnO_2/C Hybrid Triple-Layer Nanospheres as Li-ion Battery Anodes with High Stability and Rate Capability. *J. Mater. Chem. A* **2015**, *3*, 2748−2755.
(50) Górka, J.; Baggetto, L.; Keum, J. K.; Mahurin, S. M.; Mayes, R. T.; Dai, S.; Veith, G. M. The Electrochemical Reactions of SnO_2 with Li and Na: A Study Using Thin Films and Mesoporous Carbons. *J. Power Sources* **2015**, *284*, 1−9.

DOI: 10.1021/acsami.5b06512
ACS Appl. Mater. Interfaces 2015, 7, 21472−21478